Magnetic and electronic states in $(LaMnO_3)_2(SrMnO_3)_2$ superlattice exhibiting a large negative magnetoresistance

Hironori Nakao,[*] Takaaki Sudayama, Masato Kubota,[†] Jun Okamoto,[‡] Yuichi Yamasaki,[§] and Youichi Murakami
Condensed Matter Research Center and Photon Factory, Institute of Materials Structure Science, High Energy Accelerator Research Organization, Tsukuba 305-0801, Japan

Hiroyuki Yamada and Akihito Sawa
National Institute of Advanced Industrial Science and Technology, Tsukuba, Ibaraki 305-8565, Japan

Kazuaki Iwasa
Department of Physics, Tohoku University, Sendai 980-8578, Japan

(Received 30 July 2015; revised manuscript received 31 October 2015; published 7 December 2015)

Magnetic and electronic states in $(LaMnO_3)_2(SrMnO_3)_2$ superlattices fabricated on an $(LaAlO_3)_{0.3}(SrAl_{0.5}Ta_{0.5}O_3)_{0.7}$ substrate, which exhibit a large nontrivial negative magnetoresistance (MR) effect, have been investigated. The crystal structure and the Mn valence state were determined using x-ray scattering measurements near the Mn K edge. These measurements revealed that the Mn valences in the $LaMnO_3$ and $SrMnO_3$ layers are 3+ and 4+, respectively; that is, valence modulation coincides with the La/Sr stacking structure. The Mn spin structure was studied by means of resonant soft x-ray scattering at the Mn $L_{2,3}$ edge and neutron magnetic scattering measurements. We succeeded in detecting a magnetic signal indicating ferromagnetism at the interface. Finally, we suggest that the origin of the MR is the competition between ferromagnetism at the interface and underlying antiferromagnetism.

DOI: 10.1103/PhysRevB.92.245104 PACS number(s): 75.70.Cn, 75.70.−i, 77.80.bn, 73.21.Cd

I. INTRODUCTION

Thin-film fabrication techniques have developed rapidly; they allow controlling layer-stacking structures in atomic-sized levels [1]. Superlattices combining different materials have been fabricated to create new physical properties and new functions. The interface state is one of the key phenomena in the superlattice system, for example, in the high-mobility electron gas at the interface and in high-T_C interface superconductivity [2,3]. In addition to the combination of the materials, the epitaxial strain from the substrate is also a key parameter in controlling the physical properties in thin-film systems [4–7]. Recently, the oxide heterostructure system has opened a new field of materials physics [8] and has shown many potential applications [9].

Superlattices composed of $LaMnO_3$ (LMO) and $SrMnO_3$ (SMO) are heavily studied superlattice systems because the manganese oxides show various interesting phenomena, including large magnetoresistance and magnetoelectric effects [10,11], which are governed by strong couplings among charge, orbital, spin, and lattice degrees of freedom. The LMO with Mn^{3+} ($3d^4$, $t_{2g}^3e_g^1$) is a Mott insulator that exhibits A-type antiferromagnetic (A-AF) order and C-type e_g orbital order [12,13]. The SMO with Mn^{4+} ($3d^3$, t_{2g}^3) is a band insulator with G-type antiferromagnetic (G-AF) order and no orbital order [14]. Koida *et al.* have investigated the $(LMO)_m(SMO)_m$ (LmSm) superlattice fabricated on a $SrTiO_3$ (STO) substrate as a stage to control Mn valence [15]. These films are composed of the same number (m) of LMO and SMO layers, and the average Mn valence is 3.5+. The Mn valence distribution is expected to be controlled by the stacking sequence. The physical properties strongly depend on the periodicity (m): superlattices with $m \leqslant 4$ have a ferromagnetic metal (FM) phase. In contrast, superlattices with $m > 4$ have a ferromagnetic insulator (FI) phase, despite the fact that LMO and SMO are both AF insulators. It is interesting that the charge transfer through the interface between LMO and SMO layers was considered the origin of the metallic conductivity [16]. L2mSm superlattices fabricated on STO substrates have also been systematically investigated [17]. These studies indicate a phase change from the FM phase to the FI phase with increasing m, which is similar to that in the LmSm system. A large magnetoresistance (MR) effect was reported for the FI phase, whereas the FM phase exhibits a small MR effect. Moreover, neutron reflectivity measurements revealed the magnetic structure in the FI phase, in which the ferromagnetism mainly exists in the LMO layer and is suppressed in the SMO layer. The interface electronic state has been investigated using a resonant soft x-ray scattering technique, and the electronic reconstruction related to the metallic state was discussed [18,19]. The Mn valence distribution of the LmSm superlattice was studied using resonant x-ray scattering at the Mn K edge [20]. The Mn valences in the LMO and SMO layers are found to be 3+ and 4+, respectively; that is, the Mn valence modulation coincides with the stacking sequence of the LMO and SMO layers. Moreover, the accuracy of the stacking sequence and the number of layers, which are essential for the interface physical properties, were improved by using a delicate fabrication technique. Finally, it was found that all of the films show the

[*]hironori.nakao@kek.jp
[†]Present address: Quantum Beam Science Center, Japan Atomic Energy Agency, Tokai 319-1195, Japan.
[‡]Present address: National Synchrotron Radiation Research Center, Hsinchu 30076, Taiwan.
[§]Present address: Department of Applied Physics and Quantum-Phase Electronics Center, The University of Tokyo, Tokyo 113-8656, Japan.

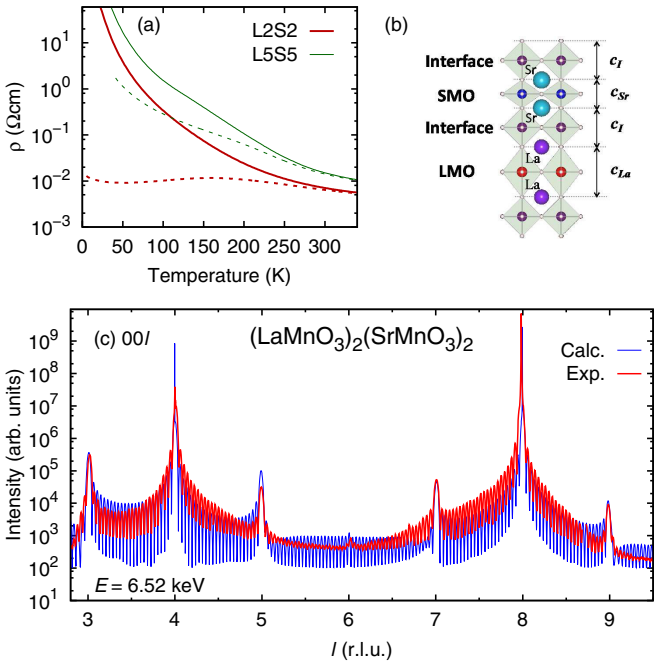

FIG. 1. (Color online) (a)Temperature dependence of resistivity for L2S2 (thick lines) and L5S5 (thin lines). Measurements under magnetic fields of 0 and 7 T are indicated by solid and dashed lines, respectively. These were taken from Ref. [21]. (b) Schematic view of the crystal structure of the L2S2 superlattice. The size of the lattice distortion is magnified for clarity. Three kinds of layers, LMO, SMO, and interface, exist in the L2S2 structure. (c) Diffraction pattern of the L2S2 superlattice, indicated by the thick solid line. The reciprocal lattice unit of the lattice constant, $c = 1.548$ nm, which is four primitive cells of perovskite, is used. The model calculation is indicated by the thin solid line.

FI phase independent of the periodicity m, although the FM phase was expected to emerge owing to the metallic state at the interface. It was made clear that the metallic conductivity in the LmSm superlattice on the STO substrate is a kind of parasitic physical property.

Yamada *et al.* examined the epitaxial strain effect for the interface state [6]. Ferromagnetism at the LMO-SMO interface was reported to appear in the isotropic MnO_6 octahedron ($c/a \sim 1$), which can realize good lattice matching with the $(LaAlO_3)_{0.3}(SrAl_{0.5}Ta_{0.5}O_3)_{0.7}$ (LSAT) substrate ($a =$ 0.387 nm), while the interface ferromagnetism with the STO substrate ($a = 0.391$ nm) is suppressed because of tensile strain from the substrate. Then, the strain effect for the LmSn superlattice fabricated using the lattice-matched LSAT substrate was systematically investigated [21]. In the case of LmSm, all of the films have insulating states; the temperature dependence of resistivity for L2S2 and L5S5 is shown in Fig. 1(a). There, superlattices with $m > 3$ are assigned to the FI phase, which indicates ferromagnetism only in the LMO layer, as observed in the L5S5 superlattice [22]. In L2S2 the magnetic transition temperature is $T_C \sim 200$ K, and the magnetization becomes about $0.26\mu_B$/Mn ($T = 5$ K and $H = 0.05$ T), which is clearly suppressed compared with the FI phase ($m > 3$). Therefore, a new AF insulator (AFI) phase is expected to be realized in the L2S2 superlattice. Moreover, a large negative MR effect was discovered, as shown in Fig. 1(a). The MR effect is much larger than that in the FI phase, and it seems to be a magnetic phase transition; the resistivity measurements for L5S5 with the FI phase are also shown in Fig. 1(a). Such a large MR effect has never been observed in an LmSn superlattice on an STO substrate, although the MR effect was reported in an LmSn superlattice on an STO substrate [15,17]. This large MR effect is sensitive to the stacking structure; that is, the MR effect is strongly suppressed in the L2S3, L3S2, and L3S3 superlattices. In L2S3, no magnetization was observed, and the magnetic transition temperature becomes roughly 240 K, which is higher than that in L2S2. Hence, the AFI phase is stabilized in L2S3. This means that L2S2 is located near the boundary between the AFI and FI phases.

Based on these phenomena, the study of magnetic structures in the L2S2 superlattice has become a major focus area. Neutron magnetic scattering measurement is a major technique for determining the magnetic structure of materials. In fact, the magnetic structures in manganite films have also been investigated using neutron magnetic scattering [23,24]. However, this investigation becomes quite difficult because of the limitations on the sample volume. Resonant magnetic soft x-ray scattering at the Mn $L_{2,3}$ edge is also an effective technique. Because the resonant signal can directly probe the $3d$ electronic state utilizing the $2p \rightarrow 3d$ dipole transition process at the $L_{2,3}$ edge, strong magnetic signals were found in the manganite superlattices [18,19,22]. In this technique, however, the observable range in scattering vector Q is too narrow to completely determine the magnetic structure. Therefore, complementary use of neutrons and soft x rays can effectively examine the magnetic state, which depends on the stacking structure and the substrate condition. In this paper, we have systematically investigated not only the magnetic state but also the valence state of the Mn ions in the L2S2 superlattice. First, the crystal structure and the Mn valence state are evaluated using an x-ray scattering technique in the hard x-ray region. Then, the magnetic structure is estimated using complementary neuron scattering and resonant soft x-ray scattering measurements. Finally, we propose that the ferromagnetic state at the interface is stabilized by the epitaxial strain.

II. EXPERIMENTS

The L2S2 superlattice was fabricated on an LSAT (001) substrate using a pulsed laser deposition technique [1]. The stacking structure of the LMO, SMO, and interface layers is shown in Fig. 1(b). The fabrication and physical properties have been reported [21]. The thickness of the film is roughly 40 nm. The out-of-plane (in-plane) lattice constant is represented by c (a). The in-plane lattice constant a matches that of the LSAT substrate ($a_{\mathrm{LSAT}} = 0.387$ nm). The uniform films of the LMO and the SMO were also fabricated to evaluate the anomalous scattering factors (ASFs) of Mn^{3+} and Mn^{4+}, respectively, and the thickness is roughly 20 nm.

Resonant x-ray scattering (RXS) and x-ray absorption spectroscopy (XAS) experiments were carried out at short-gap-undulator beam line (BL) 3A and bending magnet BL-4C at the Photon Factory (PF) at High Energy Accelerator Research Organization (KEK). Experiments were performed

on a four-circle diffractometer with σ-polarized incident x rays near the Mn K edge. The temperature was controlled using a closed-cycle He refrigerator.

A neutron magnetic scattering experiment was performed using a thermal neutron spectrometer, TOPAN, installed at beam hole 6G of the JRR-3 reactor of Japan Atomic Energy Agency (JAEA). The incident neutron energy was monochromatized to $E_i = 13.5$ meV ($\lambda = 0.246$ nm) by the 002 reflection of a pyrolytic-graphite monochromator. The pyrolytic-graphite analyzer, set at the 002 reflection, and the pyrolytic-graphite filter were used to eliminate higher harmonics. No collimator was used to obtain sufficient scattering intensity from the film. The 12 films were used, and the total area is roughly 30×15 mm^2. We characterized the physical properties of all samples, and all properties show large MR phenomena, as shown in Fig. 1(a).

Resonant soft x-ray scattering (RSXS) and XAS experiments were performed near the Mn $L_{2,3}$ edge at BL-16A and 19B in the PF using an in-vacuum two-circle diffractometer [25,26]. The π-polarized incident x ray was used; the intensities integrating over both π and σ final-state polarizations were measured [see the inset in Fig. 6(b) below]. A magnetic field of roughly 0.4 T perpendicular to the scattering plane was applied; permanent magnets were used to align the magnetic domains.

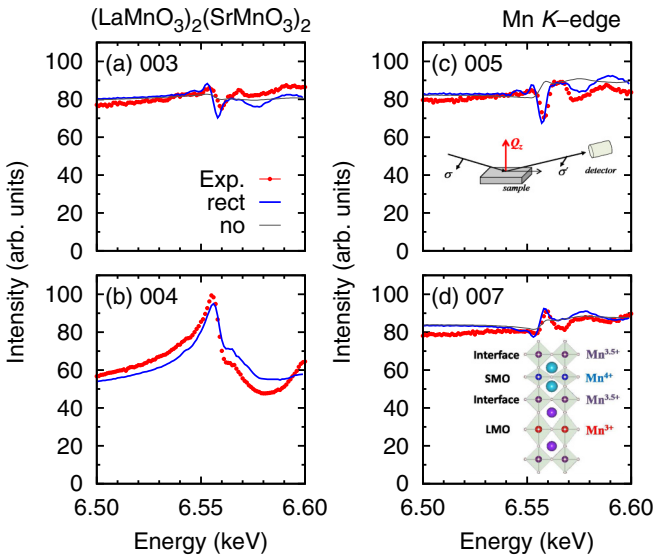

FIG. 2. (Color online) Energy dependence of scattering intensities of (a) the 003, (b) 004, (c) 005, and (d) 007 reflections. See Fig. 1 regarding the intensity ratios among the reflections since the intensities are roughly scaled. Model calculations are indicated by a thick solid line ("rect" model) and a thin solid line ("no" model). See the text for the details of these models. The inset in (c) shows the schematic view of the experimental configuration. The inset in (d) shows the Mn valence states of the rect model.

III. RESULTS AND DISCUSSION

Resonant x-ray scattering measurements have been performed near the Mn K edge to evaluate the Mn valence states in the L2S2 superlattice. The diffraction pattern along the stacking direction is shown in Fig. 1(c); the reflections are indexed by the lattice constant, $c = 1.548$ nm, of the superstructure containing four layers of the perovskite unit cell in the L2S2 structure. The 004 and 008 reflections are the fundamental peaks of the perovskite unit cell, which reflects the lattice-constant-averaged four layers of the perovskite; that is, it is the averaged lattice constant, $c_{\rm ave} = c/4 = 0.387$ nm. The sharp peaks on the fundamental peaks correspond to the Bragg reflections of the LSAT substrate. This result implies that the lattices of L2S2 and the substrate match well. The superlattice peaks exist between the fundamental peaks, which is attributed to the superstructure. Moreover, the peaks due to the Laue function are clearly observed, even around the 006 reflection. These peak structures are much more clearly observed than those of superlattices fabricated on the STO substrate [20].

The energy dependence of the scattering intensity $I(E, Q)$ was measured near the Mn K edge at the reflection positions shown in Fig. 2. The energy spectra show a marked energy dependence, which is attributed to the ASF of Mn ions. At the superlattice reflections, strong resonating signals were observed near the Mn K-edge energy. The observed spectra are similar to those reported in the film on the STO substrate [20]. The intensity of the resonant signal mainly reflects the Mn valence state in the LMO and the SMO layers. Thus, it indicates that the Mn valence distribution is also similar to those in the superlattice on the STO substrate.

To determine the crystal structure of the superlattice, we construct a simple structural model of L2S2, which has the lattice constant parameters of LMO ($c_{\rm La}$), STO ($c_{\rm Sr}$), and interface (c_I) layers, as shown in Fig. 1(b). In this paper, the lattice relaxation parameter [20] near the interface is not used because the lattice constants of four layers are enough to be treated in the L2S2 superlattice. This structural model is the same as that used in Ref. [20]. Namely, the parameters are the lattice constants of (La,Sr)MnO_3 of each layer, and the atomic positions in the perovskite unit cell are kept. Here the relations $c_{\rm ave} = (c_{\rm La} + c_{\rm Sr})/2 = c_I$, $c = c_{\rm La} + c_{\rm Sr} + 2c_I$, and $\Delta c = (c_{\rm La} - c_{\rm Sr})/2$ are used. The model calculation with $c_{\rm ave} = 0.387$ nm and $\Delta c = 0.003$ nm is shown in Fig. 1(c). The peak positions, superlattice intensities, and the Laue function are well explained by the calculation. The result is consistent with the unique structural character of an L2S2 superlattice on an LSAT substrate; namely, the LMO (SMO) layer is realized to be under compressive (tensile) strain. The previous study of the L2S2 superlattice on the STO considered a small amount of A-site cation diffusion near the interface [20], because intensity of a superlattice reflection, which is far from the fundamental peak position, was lower than the expected value in model calculation. In this case, on the other hand, the intensity is well explained by the model calculation even around the 006 reflection. Hence, there is no diffusion of A-site cations within the experimental error. For precise estimation of the structural parameters, we need to observe in the wider Q region. However, the model structure is enough to estimate the Mn valence state because the signal reflecting the valence state is strongly observed in the low-angle region. Thus, we estimated the L2S2 structure by utilizing this simple structural model.

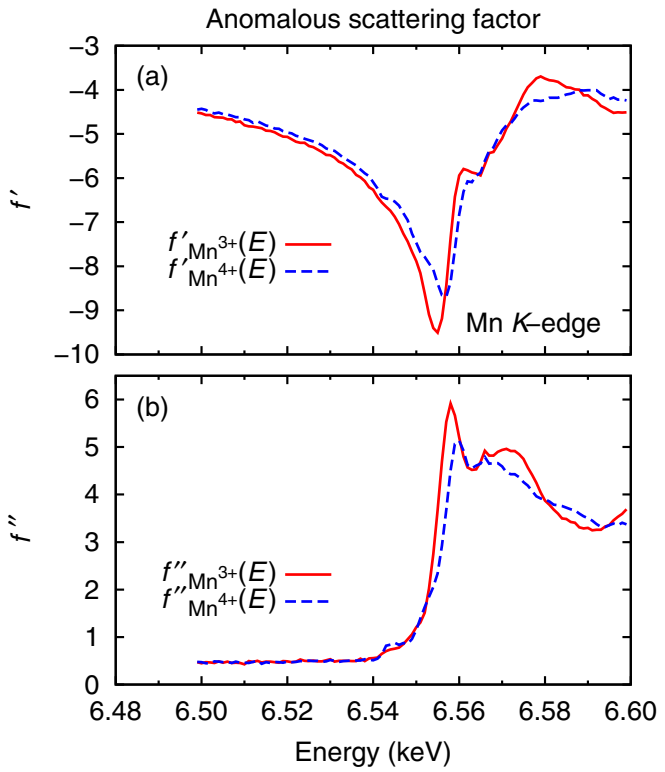

FIG. 3. (Color online) Anomalous scattering factors (a) $f'(E)$ and (b) $f''(E)$ near the Mn K-edge energy, which were estimated using the simple LMO (Mn^{3+}) and SMO (Mn^{4+}) films as shown by solid and dashed lines, respectively. The inset in (b) shows the schematic view of the experimental configuration.

ASFs, f' and f'', of Mn^{3+} and Mn^{4+} are necessary to calculate $I(E,Q)$. In a previous study, however, the fluorescence signal from the film was weak; therefore, the ASFs of Mn^{3+} and Mn^{4+} could not be determined [20]. In this study, we have succeeded in detecting absorption spectra $\mu(E)$ of simple LMO and SMO films using a fluorescence yield (FY) mode. Here we determine the in-plane component of the ASF with the experimental configuration (inset of Fig. 3); this means that the polarization vector of the incident x ray is parallel to the film's surface. The in-plane component of ASF mainly reflects the valence state because there is no difference in the Mn-O bonding along the in-plane direction in epitaxially grown LMO and SMO films with the same in-plane lattice constant (a_{LSAT}). The observed $\mu(E)$ was transformed into the imaginary part of the anomalous scattering factor $f''(E)$ using the relation $f''(E) = \frac{m_e E}{2Nhe^2}\mu(E)$, where m_e is the electron mass, e is the electron charge, N is the atomic number density, and h is Plank's constant [27]. The obtained $f''(E)$ spectra are shown in Fig. 3(b). $f'(E)$ was calculated from the Kramers-Krönig transformation of $f''(E)$, as shown in Fig. 3(a). There is an energy shift reflecting the Mn valence state, the so-called chemical shift, of roughly 2 eV. The peak at the edge of $f''_{Mn^{3+}}$ is higher than that of $f''_{Mn^{4+}}$. The obtained ASFs, f' and f'', are consistent with those obtained from the bulk LMO and SMO compounds [20]. We believe that realistic ASFs can be obtained here.

The energy dependence $I(E,Q)$ is calculated to evaluate the Mn valence state using the simple structural model and the obtained ASFs of Mn^{3+} and Mn^{4+}. The Mn valence distribution models, "rect" and "no" models [20], are considered for the L2S2 superlattice. In the "rect" model, the Mn valence in the LMO (SMO) layer is 3+ (4+), and the valence becomes 3.5+ at the interface, as shown in the inset of Fig. 2(d). In the "no" model, the Mn valence is uniform at 3.5+; that is, it is a charge-disordered model. Figure 2(b) shows the energy dependence of the scattering intensity for the 004 fundamental reflection. The spectrum is explained better than those in the literature, [20] because more realistic ASFs are used in this calculation. The $I(E,Q)$ at the superlattice reflections are calculated using the "rect" and the "no" models, as shown in Fig. 2. The rect model can accurately explain the peak structures near the Mn K edge. This model elucidates that the Mn valences in the LMO and SMO layers are 3+ and 4+, respectively; that is, the Mn valence is fully controlled by the La/Sr stacking structure, as shown in the inset of Fig. 2(d). Namely, the charge transfer does not occur through the interface between the LMO and SMO layers within the experimental error. Such an interface state was also reported in previous studies [15–17].

The magnetic structure in the L2S2 superlattice has been investigated using neutron magnetic scattering measurements. It is difficult to observe the signal from the film separately from the signal from the substrate peak because the lattices of the film and substrate are similar. Therefore, no signal from the L2S2 superlattice could be observed at room temperature. The temperature dependence of the peak profiles was measured to evaluate the magnetic signal. Figure 4(b) shows the peak profiles of the 002 reflection; a peak structure emerges below T_C. On the other hand, no peak structure was observed for the 003 reflection, as shown in Fig. 4(a). No magnetic signal was observed for the 001 reflection [28]. The temperature dependence of peak intensity was measured precisely for the 002 reflection, as shown in Fig. 4(c). The dependence indicates a gradual increase below T_C and scales with the square of the magnetization [20]. Therefore, we succeeded in detecting the magnetic signal from the L2S2 superlattice for the 002 reflection. As a result, the magnetic structure has periodicity with two layers of perovskite unit cell, and the periodicity with the four layers cannot be detected within this experimental error. Namely, the magnetic structure in the L2S2 is different from that in the L5S5, where ferromagnetism is present mainly in the LMO layer [22].

Two magnetic structure models are considered here. One model is A-AF, which has a ferroic arrangement in the ab plane and an antiferroic arrangement along the stacking direction, c, as shown in Fig. 5(a). This model is consistent with the existence of the magnetic signal in the 002 reflection. Such an A-AF was reported in the manganite superlattice on an STO substrate [23]. In this model, the magnetic signal in the 001 and 003 (odd) reflections, which reflects the difference of the moment size between LMO (Mn^{3+}, $3d^4$) and SMO (Mn^{4+}, $3d^3$) layers, is also observable. The other model is interface ferromagnetism, which also corresponds to the magnetic signal in the 002 reflection, as shown in Fig. 5(b). In this model, we consider that the LMO and SMO layers have the antiferroic arrangement in the ab plane, i.e., G-AF and C-AF, although the

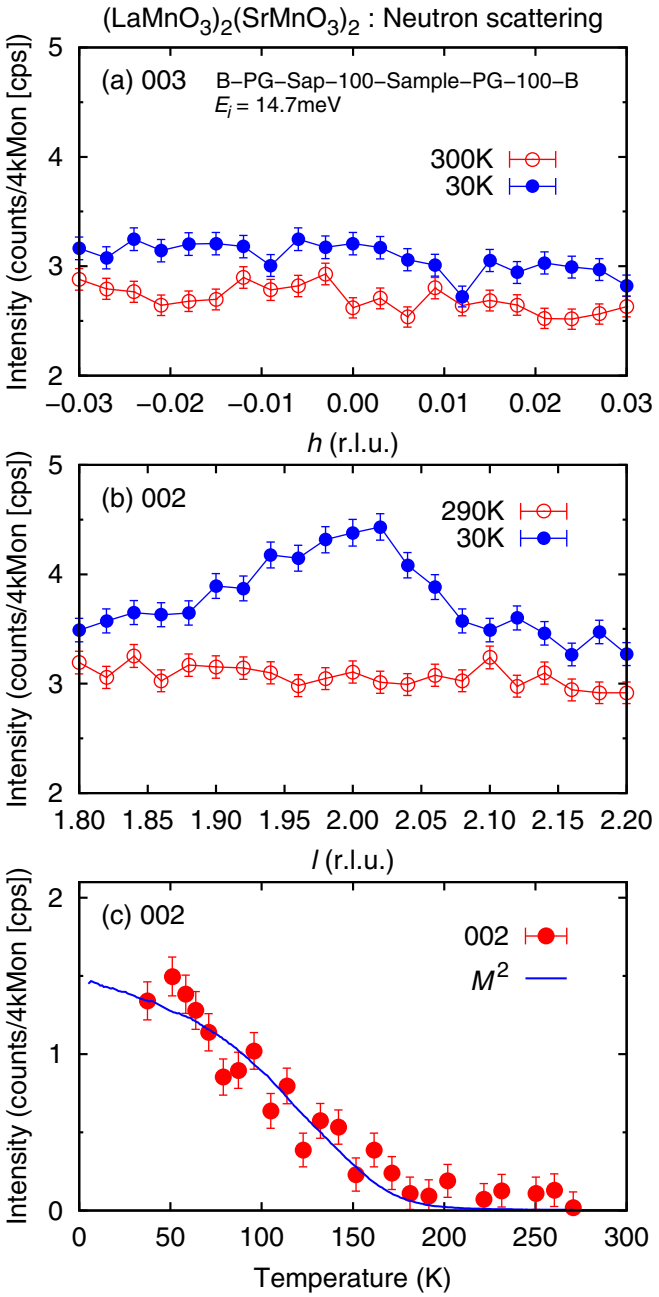

FIG. 4. (Color online) Peak profiles for (a) 003 and (b) 002 reflections along the h and l directions, respectively. (c) Temperature dependence of peak intensity of the 002 reflection; the baseline is shifted to allow comparison with the magnetization data. The square of the magnetization [21] M^2 is indicated by a solid line.

AF state in the ab plane is not elucidated by the observation. In the model, no magnetic signal is expected to appear in the odd reflection since there is no net moment in the ab plane of the underlying AF. Finally, the interface ferromagnetism is considered, as the canted component in the AF state, to be the origin of the magnetization, as shown in Fig. 5(c). To determine the magnetic structure, therefore, it is important to confirm whether the magnetic signal exists in the odd reflection or not. However, confirmation is difficult because of the insufficient neutron flux because the intensity of the odd reflection is expected to be weaker than that of the 002 reflection.

To clarify the magnetic structure of the L2S2 superlattice, an RSXS measurement was performed to investigate the magnetic signal of the 001 reflection. Using the RSXS technique, the magnetic signals were easily measured in a manganite superlattice system [18,19,22]. In fact, the strong magnetic signals, which reflect the ferromagnetic moment in the LMO layer (roughly $1\mu_B$/Mn), were observed in the L5S5 superlattice [22]. Therefore, we find that the magnetic signal is detectable in the 001 reflection in the A-AF case because the difference between the Mn^{3+} and Mn^{4+} magnetic moment sizes is expected to be roughly $1\mu_B$. On the other hand, the 002 reflection cannot be observed by the RSXS because of the limitation of the observable Q range. The XAS of the L2S2 superlattice was measured using the FY mode, as shown in Fig. 6(a). The absorption structure at the Mn $L_{2,3}$ edge was clearly observed. The energy dependence of the scattering intensity was measured for the 001 reflection near the Mn $L_{2,3}$ edge, as shown in Fig. 6(b). The spectrum indicates a strong resonating feature near the Mn $L_{2,3}$ edge. As discussed in the RXS study at the Mn K edge, the resonant signal above T_C mainly reflects the valence difference between the LMO and SMO layers.

By using the ASFs of Mn^{3+} and Mn^{4+} near the Mn $L_{2,3}$ edge reported in the previous study [22], the energy spectrum was calculated with the rect valence distribution model utilizing the same procedure at the Mn K edge. The calculated resonant intensity [i.e., I(640.4 eV)/I(634.0 eV)] is weaker than that of the observation. It means that the valence difference between the LMO and the SMO layers is larger than one electron. This overestimation may be caused by the insufficient accuracy of the ASFs at the Mn $L_{2,3}$ edge. Hence, the quantitative evaluation is difficult so far. However, this result also supports that the Mn valences in the LMO and SMO layers are 3+ and 4+, respectively; that is, valence modulation coincides with the La/Sr stacking structure. Then, the energy spectrum shows almost no temperature dependence, although the magnetic signal is expected to be observed below T_C in the A-AF case. No temperature dependence of the energy spectrum indicates that the Mn valence modulation does not change upon the onset of the magnetic order. To detect small changes in the energy spectrum, we measured the temperature dependence of the intensity ratio between the intensities at resonant and nonresonant energies. However, our results do not indicate any variation associated with the magnetism near T_C, as shown in Fig. 6(c). This result shows that the no component of the A-AF structure exists in the L2S2 superlattice within this experimental error. Finally, we conclude that the 002 reflection is the magnetic signal, which reflects the interface ferromagnetism. This is also consistent with the fact that the temperature dependence of the 002 reflection intensity scales well with the square of the magnetization.

The structural character of the superlattice fabricated on the LSAT substrate indicates that the LMO layer is under compressive strain, the SMO layer is under tensile strain, and the superlattice fabricated on the STO is under strong tensile strain. This result reflects lattice matching between the manganite superlattice and the LSAT substrate. The epitaxial strain effect for the electronic state in the manganite film

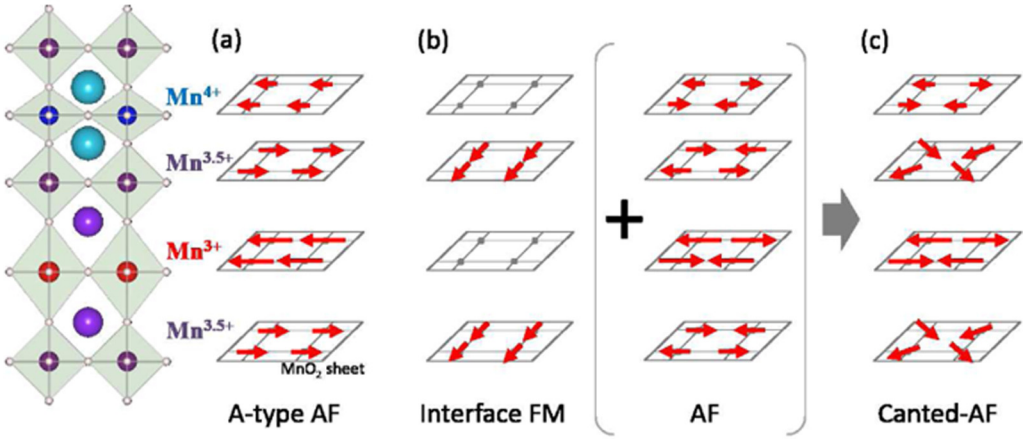

FIG. 5. (Color online) Magnetic structure models. (a) A-type antiferromagnetism (A-AF). The difference between the magnetic moment sizes and the canted components is magnified for clarity. (b) Interface ferromagnetism and underlying antiferromagnetism. The underlying AF is drawn in parentheses. (c) Canted-AF structure, in which the interface FM and the underlying AF are superimposed.

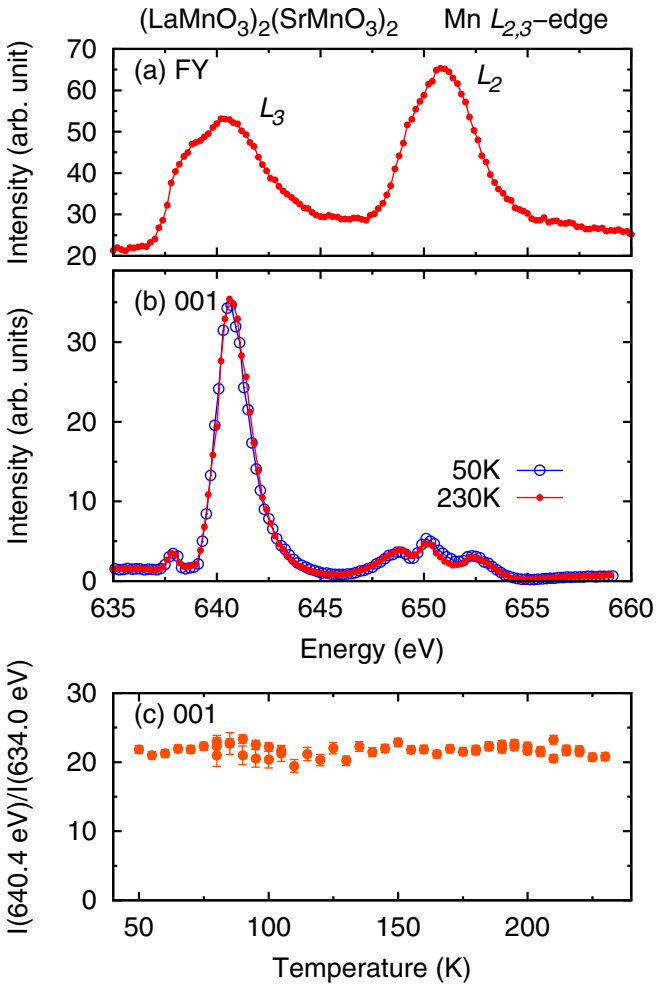

FIG. 6. (Color online) (a) XAS spectrum of the L2S2 superlattice measured in the FY mode. The intensity at the L_3 edge is suppressed because of the self-absorption effect. (b) Energy dependence of the scattering intensities in the 001 reflection. (c) Temperature dependence of the intensity ratios between the intensity at 640.4 eV and that at 634.0 eV.

was studied experimentally and theoretically [4,5]. The A-AF, C-AF, and ferromagnetic phases were reported to emerge depending on the strain field of the substrates. For example, under a compressive strain field, the ferro-type $3z^2$-r^2 orbital ordering is stabilized; then, AF coupling in the ab plane is dominated by the superexchange (SE) interaction between the t_{2g} and t_{2g} orbitals, which is similar to the AF interaction along the c direction in $LaMnO_3$. Along the stacking direction, the ferromagnetic interaction is expected because of the double-exchange (DE) mechanism. Finally, the C-AF phase is stabilized under a compressive strain field. In the same way, under a tensile strain field, the ferro-type x^2-y^2 orbital ordering is stabilized, and the A-AF phase is realized. In fact, the A-AF phase of this mechanism was experimentally reported in an LmS2m superlattice on an STO substrate with strong tensile strain [23].

We examine the influence of the strain effect on the magnetic structure in the L2S2 superlattice. The LMO layer is under a compressive strain field, and thus, the occupancy of the $3z^2$-r^2 orbital is enhanced. Then, the magnetic interaction is expected to be C-AF type. In the SMO layer, there is no e_g orbital because of the Mn^{4+}. Therefore, the AF coupling for all directions is dominated by the SE interaction between the t_{2g} and t_{2g} orbitals, and the magnetic interaction becomes G-AF type, as in bulk SMO. Thus, the AF magnetisms are expected in both the LMO and SMO layers. Both the C-AF and G-AF magnetic structures have no net magnetic moment in the ab plane. Hence, the AF magnetic structures are consistent with observing no magnetic signal in the odd reflection. Then, the AF magnetic structure is realized if the magnetic interaction at the interface is governed by AF coupling due to the SE interaction. This underlying AF corresponds to the G-AF magnetic structure, as shown in Fig. 5(b). The G-AF magnetic structure is consistent with the insulative behavior, while the A-AF phase is associated with the metallic state. In order to determine the underlying AF magnetic structure, it is necessary to observe the magnetic signal at $\frac{1}{2}\frac{1}{2}2$ reflection in the notation used here. However, the signal reflecting the short-range order in the B-site of the LSAT substrate is strongly observed near the peak position [24]. Therefore, it is difficult

to confirm the underlying AF magnetic structure by using the neutron magnetic scattering. In the RSXS measurement, this magnetic structure is impossible to measure because the Q vector is too large for the observation. As a result, it has been difficult to confirm the presence of the AF magnetic structure experimentally. At the interface, on the other hand, the isotropic octahedron is realized because of the lattice matching, and the disordered e_g orbital state is expected. Therefore, the ferromagnetic state is expected to be induced at the interface, as discussed in the literature [6]. Consequently, the ferromagnetic state induced at the interface competes with the AF states in both the LMO and SMO layers and is expected to be the canted component at the interface, as shown in Fig. 5(c). We believe that the competition among underlying AF states and the ferromagnetism at the interface is the origin of the large MR effect in the L2S2 superlattice.

In conclusion, we have investigated the spin, charge, and orbital states of Mn ions in an L2S2 superlattice on a lattice-matched LSAT substrate using both x-ray and neutron scattering measurements. We confirmed that the LMO (SMO) layer is under compressive (tensile) strain and that the Mn valences in the LMO and SMO layers are 3+ and 4+, respectively. The interface ferromagnetism and the antiferromagnetic structure in the ab plane of the LMO and SMO layers are clearly elucidated based on observations of the magnetic reflections. We also suggested that competition among the AF states and the ferromagnetic state at the interface is the origin of the large MR effect in the L2S2 superlattice. One such unique magnetic state is realized via control of the epitaxial strain in the superlattice. To clarify the microscopic origin of the MR effect, we must further investigate the magnetic field effects in the L2S2 superlattice. Further systematic study of the electronic and magnetic states is also important for the LmSn superlattice. In future studies, we will discuss the magnetic interaction between Mn ions, for which the precise crystal structure should be determined.

ACKNOWLEDGMENTS

We wish to thank H. Sagayama, R. Kumai, T. Arima, and S. Ishihara for fruitful discussions. This research was partially supported by the JSPS KAKENHI Grant [Grants No. 16104005, No. 16684008, No. 20102005, No. 21224008, No 23244068, No 24654080, No. 25286090, and No. 15H05885 (J-Physics)], the Funding Program for World-Leading Innovative R&D on Science and Technology (FIRST), and the JST, Invitation for Applications for the Strategic Basic Research Programs (CREST). This study has been performed under the Photon Factory Program Advisory Committee (Proposals No. 2009S2-008, No. 2012S2-005, No. 2015G548, and No. 2015PF-BL-19B) and under the User Program for neutron scattering conducted by ISSP, The University of Tokyo.

[1] M. Kawasaki, M. Izumi, Y. Konishi, T. Manako, and Y. Tokura, Mater. Sci. Eng. **63**, 49 (1999).
[2] A. Ohtomo and H. Y. Hwang, Nature (London) **427**, 423 (2004).
[3] A. Gozar, G. Logvenov, L. F. Kourkoutils, A. T. Bollinger, L. A. Giannuzzi, D. A. Muller, and I. Bozovic, Nature (London) **455**, 782 (2008).
[4] Y. Konishi, Z. Fang, M. Izumi, T. Manako, M. Kasai, H. Kuwahara, M. Kawasaki, K. Terakura, and Y. Tokura, J. Phys. Soc. Jpn. **68**, 3790 (1999).
[5] Z. Fang, I. V. Solovyev, and K. Terakura, Phys. Rev. Lett. **84**, 3169 (2000).
[6] H. Yamada, M. Kawasaki, T. Lottermoser, T. Arima, and Y. Tokura, Appl. Phys. Lett. **89**, 052506 (2006).
[7] A. Frano, E. Schierle, M. W. Haverkort, Y. Lu, M. Wu, S. Blanco-Canosa, U. Nwankwo, A. V. Boris, P. Wochner, G. Cristiani, H. U. Habermeier, G. Logvenov, V. Hinkov, E. Benckiser, E. Weschke, and B. Keimer, Phys. Rev. Lett. **111**, 106804 (2013).
[8] H. Y. Hwang, Y. Iwasa, M. Kawasaki, B. Keimer, N. Nagaosa, and Y. Tokura, Nat. Mater. **11**, 103 (2012).
[9] S. M. Wu, S. A. Cybart, P. Yu, M. D. Rossell, J. X. Zhang, R. Ramesh, and R. C. Dynes, Nat. Mater. **9**, 756 (2010).
[10] M. Imada, A. Fujimori, and Y. Tokura, Rev. Mod. Phys. **70**, 1039 (1998).
[11] T. Kimura, T. Goto, H. Shintani, K. Ishizaka, T. Arima, and Y. Tokura, Nature (London) **426**, 55 (2003).
[12] E. O. Wollan and W. C. Koehler, Phys. Rev. **100**, 545 (1955).
[13] Y. Murakami, J. P. Hill, D. Gibbs, M. Blume, I. Koyama, M. Tanaka, H. Kawata, T. Arima, Y. Tokura, K. Hirota, and Y. Endoh, Phys. Rev. Lett. **81**, 582 (1998).
[14] T. Takeda and S. Ohara, J. Phys. Soc. Jpn. **37**, 275 (1974).
[15] T. Koida, M. Lippmaa, T. Fukumura, K. Itaka, Y. Matsumoto, M. Kawasaki, and H. Koinuma, Phys. Rev. B **66**, 144418 (2002).
[16] C. Lin, S. Okamoto, and A. J. Millis, Phys. Rev. B **73**, 041104 (2006).
[17] A. Bhattacharya, S. J. May, S. G. E. te Velthuis, M. Warusawithana, X. Zhai, B. Jiang, J.-M. Zuo, M. R. Fitzsimmons, S. D. Bader, and J. N. Eckstein, Phys. Rev. Lett. **100**, 257203 (2008).
[18] S. Smadici, P. Abbamonte, A. Bhattacharya, X. Zhai, B. Jiang, A. Rusydi, J. N. Eckstein, S. D. Bader, and J.-M. Zuo, Phys. Rev. Lett. **99**, 196404 (2007).
[19] S. Smadici, B. B. Nelson-Cheeseman, A. Bhattacharya, and P. Abbamonte, Phys. Rev. B **86**, 174427 (2012).
[20] H. Nakao, J. Nishimura, Y. Murakami, A. Ohtomo, T. Fukumura, M. Kawasaki, T. Koida, Y. Wakabayashi, and H. Sawa, J. Phys. Soc. Jpn. **78**, 024602 (2009).
[21] H. Yamada, P.-H. Xiang, and A. Sawa, Phys. Rev. B **81**, 014410 (2010).
[22] M. Kubota, H. Yamada, H. Nakao, J. Okamoto, Y. Yamasaki, A. Sawa, and Y. Murakami, Jpn. J. Appl. Phys. **53**, 05FH07 (2014).
[23] S. J. May, P. J. Ryan, J. L. Robertson, J.-W. Kim, T. S. Santos, E. Karaperova, J. L. Zarestkly, X. Zhai, S. G. E. te Velthuis, J. N. Eckstein, S. D. Bader, and A. Bhattacharya, Nat. Mater. **8**, 892 (2009).
[24] H. Nakao, H. Yamada, A. Sawa, K. Iwasa, J. Okamoto, T. Sudayama, Y. Yamasaki, and Y. Murakami, Solid State Commun. **185**, 18 (2014).

[25] J. Okamoto, K. Horigane, H. Nakao, K. Amemiya, M. Kubota, Y. Murakami, and K. Yamada, J. Phys. Conf. Ser. **425**, 202003 (2013).

[26] H. Nakao, Y. Yamasaki, J. Okamoto, T. Sudayama, Y. Takahashi, K. Kobayashi, R. Kumai, and Y. Murakami, J. Phys. Conf. Ser. **502**, 012015 (2014).

[27] J. O. Cross, M. Newville, J. J. Rehr, L. B. Sorensen, C. E. Bouldin, G. Watson, T. Gouder, G. H. Lander, and M. I. Bell, Phys. Rev. B **58**, 11215 (1998).

[28] The peak structure exists at the 001 reflection position. However, it indicates no temperature dependence.